APPLIED GEOPHYSICS, Vol.12, No.3 (September 2015), P. 334-342, 15 Figures.
DOI:10.1007/s11770-015-0512-2

A new approach for salt dome detection using a 3D multidirectional edge detector*

Asjad Amin[1] and Mohamed Deriche♦[1]

Abstract: Accurate salt dome detection from 3D seismic data is crucial to different seismic data analysis applications. We present a new edge based approach for salt dome detection in migrated 3D seismic data. The proposed algorithm overcomes the drawbacks of existing edge-based techniques which only consider edges in the x (crossline) and y (inline) directions in 2D data and the x (crossline), y (inline), and z (time) directions in 3D data. The algorithm works by combining 3D gradient maps computed along diagonal directions and those computed in x, y, and z directions to accurately detect the boundaries of salt regions. The combination of x, y, and z directions and diagonal edges ensures that the proposed algorithm works well even if the dips along the salt boundary are represented only by weak reflectors. Contrary to other edge and texture based salt dome detection techniques, the proposed algorithm is independent of the amplitude variations in seismic data. We tested the proposed algorithm on the publicly available Netherlands offshore F3 block. The results suggest that the proposed algorithm can detect salt bodies with high accuracy than existing gradient based and texture-based techniques when used separately. More importantly, the proposed approach is shown to be computationally efficient allowing for real time implementation and deployment.
Keywords: Salt dome, seismic interpretation, 3D edge detection, 3D Sobel, multidirectional edge detector

Introduction

The properties of waves change as they propagate through rocks and fluids, and seismic data are obtained from reflection of the waves at subsurface. Wave reflections received by the surface sensors contains important geological information which is used to identify:

- rock layer and faults,
- structure and structural features,
- salt domes and other bodies,
- fluid presence,
- oil and gas traps,
- rock properties, etc.

Data analysis is performed by either human experts or computer-aided systems. Seismic data interpretation is a difficult task because the data contain noise owing

Manuscript received by the Editor August 12, 2015; revised manuscript received September 17, 2015.
*The work presented in this paper has been supported by the Center for Energy and Geo Processing (CeGP) at King Fahd University of Petroleum & Minerals (KFUPM), under Project no. GTEC 1401-1402.
1. Center for Energy and Geo Processing (CeGP) at King Fahd University of Petroleum & Minerals.
♦Corresponding author: Mohamed Deriche (Email: mderiche@kfupm.edu.sa)

to multiple reflections and wave refraction or noise is simply random, Manual seismic interpretation is reliable but slow, and it requires a large well-trained and experienced workforce Alternatively, automated interpretation systems with input from an expert are used. This improves accuracy and reduces interpretation time.

Major accumulations of oil and gas are associated with salt domes owing to their impermeability. Salt domes are largely subsurface cylinder-like geologic structures (Brown et al., 2004). The detection of salt domes is a difficult and time consuming task, especially in the case of 3D seismic data volumes (Berthelot et al., 2013). Most automated and semi-automated salt dome detection algorithms are based on edge detection methods (Jing et al., 2007; Aqrawi et al., 2011), normalized cuts image segmentation (NCIS) (Lomaskand and Biondi, 2003; Lomask et al., 2004; Lomask et al. 2006), active contour models (Zhang and Halpert, 2012; Haukas et al., 2013), and texture attributes (Berthelot et al., 2012; Berthelot et al., 2013).

The NCIS algorithm discussed by Shi and Malik (2000) detects salt domes by solving a global optimization problem, and therefore is less sensitive to local discontinuities. The method was used for the detection of salt boundaries by Lomask and Biondi (2003), Lomask et al. (2004), and Lomask et al. (2006). NCIS based algorithms are computationally expensive and are therefore not suitable for real time seismic interpretation.

Salt boundary segmentation methods based on the active contour models(ACM) (e.g., Zhang and Halpert, 2012; Haukas et al., 2013), combine the input from an expert with automatic segmentation. The initial boundary information is provided by a human expert. The refined boundary is found based on such initial information and numerous numerical iterations to optimize a certain cost function.

Salt dome boundaries are often characterized by changes in texture rather than reflectivity. Therefore, use of only boundary-sensitive attributes such as instantaneous amplitude may result in incorrect interpretation. Salt dome detection methods using texture attributes have been discussed by Berthelot et al. (2012), Berthelot et al. (2013), and Hegazy and AlRegib (2014). The challenge with texture based schemes is to obtain the most important texture features or attributes. This may also require heavy computation (Berthelot et al., 2013).

On the other hand, edge-detection-based techniques (Jing et al., 2007; Aqrawi et al., 2011) are simple and very useful in detecting salt dome boundaries. Jing et al. (2007) implemented general form of the Sobel algorithm by applying masks with different weights and then combining weighted samples. The combined samples provide information about dissimilarities in an image along any direction. The Sobel edge detector belongs to a general class of edge detection algorithm based on a simple formulation of derivatives using weighting masks. In the case of the 2D Sobel operator, the first mask detects discontinuities in one direction, whereas the second mask detects dissimilarities in another direction. The boundary of the salt dome is tracked by combining two dissimilarity maps. No normalization is performed, the scheme works well only when seismic data exhibits small amplitude variations of comparable magnitude in two directions.

Aqrawi et al. (2011) proposed a salt body detection algorithm based on the 3D formulation of the Sobel operator. The latter is combined with amplitude normalization and dimension weighting. The normalization minimizes variations between low and high amplitudes. The weighting is used to prevent any horizontal artifacts that may appear owing to vertical gradients. The scheme starts by estimating the structural dip that maximizes the trace to trace correlation. The second step is to compute the discontinuities using the dip. The third step involves the 3D Sobel edge detector. We used a $3 \times 3 \times 3$ operator. The proposed 3D Sobel edge detector with normalization works even if seismic data shows amplitude variations. Other edge detection techniques for 3D data were discussed by Xu et al. (2015), Li et al. (2014), and Wang et al. (2009).

We propose a robust framework for salt dome detection based on a new formulation of the 3D edge detector. Most existing 2D-edge-based techniques consider edges in x (crossline) and y (inline) directions, whereas 3D edge-based techniques consider edges in x (crossline), y (inline), and z (time) directions. Such schemes often fails to accurately trace the salt dome boundary along diagonals. Thus, we propose two new 3D Sobel operators that compute the edges along diagonal directions. We combine the diagonal edges and the edges along the x, y, and, z directions to overcome the weaknesses of existing amplitude-based salt dome detection methods. The proposed algorithm produces finer results compared to existing edge-based and texture-attributes-based salt dome detection methods when used separately.

The proposed salt dome detection algorithm

The proposed algorithm works by computing the edge map of 3D seismic data. The algorithm considers diagonal edges and the edges in x, y, and z directions. It starts by normalizing the available data to enhance the salt dome edges. Then, we compute the gradient magnitudes in the x, y, z directions, and diagonal directions. We get the outline of the salt boundary by combining and thresholding all the edge maps. Figure 1 shows the flowchart for the proposed algorithm.

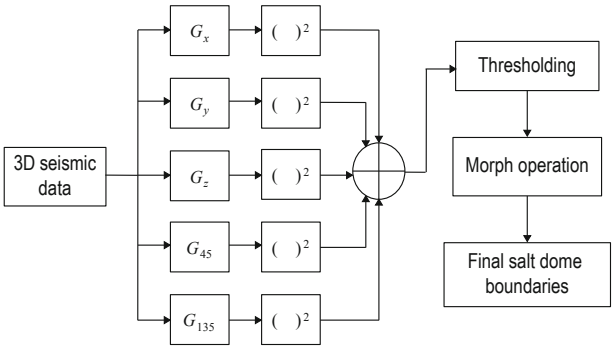

Fig. 1 The workflow of the proposed algorithm.

The 2D Sobel edge detector

Edge detection is one of the most important image processing tasks used to detect pixels intensity variations in an image. Edge detection can be used for the accurate estimation of dissimilarities caused by faulting or stratigraphic variations.

The Sobel edge detector, which uses the first derivative, is the most common operator used in the detection of salt domes. The Sobel operator is a differentiation operator which computes the gradient of the image intensity function. The Sobel edge detector in 2D computes spatial gradients of a 2D image and enhances regions of high frequency that represent edges. The discrete gradient equations for a 3 × 3 Sobel edge detector in the x and y directions are given as:

$$G_x=\{g(x+1,y+1)+2g(x+1,y)+g(x+1,y+1)\} -\{g(x-1,y-1)+2g(x-1,y)+g(x-1,y+1)\}, \quad (1)$$

$$G_y=\{g(x-1,y+1)+2g(x,y+1)+g(x+1,y+1)\} -\{g(x-1,y-1)+2g(x,y-1)+g(x+1,y-1)\}, \quad (2)$$

where $g(x,y)$ is the amplitude value at x and y position. The magnitude of the total gradient is given as:

$$G=\sqrt{G_x^{\,2}+G_y^{\,2}}. \quad (3)$$

The convolution operators for the Sobel edge detector in the x direction and y directions are given as:

$$S_x=\begin{bmatrix}-1 & 0 & 1\\ -2 & 0 & 2\\ -1 & 0 & 1\end{bmatrix}, \quad (4)$$

$$S_y=\begin{bmatrix}-1 & -2 & -1\\ 0 & 0 & 0\\ 1 & 2 & 1\end{bmatrix}. \quad (5)$$

From the above equations, we note that the first mask detects discontinuities in one direction and the second mask detects discontinuities in the other direction. The boundary of the salt dome is tracked by combining the two dissimilarity maps into a single magnitude map. An example of the resulting salt boundary is shown in Figure 2.

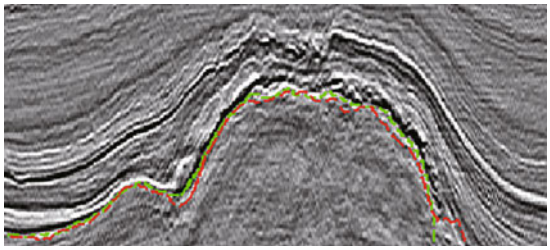

Fig.2 Salt boundary detected for the Inline # 111 using 2D Sobel edge detector.

Other edge detection based techniques such as the Prewitt edge detector (Gonzalez and Richard, 2002), and the Scharr edge detector can also be used to detect salt boundaries. Like the Sobel operator, the Prewitt operator is also a first order edge operator but using different kernels. The Prewitt gradients, in the x and y directions, are given as:

$$S_x=\begin{bmatrix}-1 & 0 & 1\\ -1 & 0 & 1\\ -1 & 0 & 1\end{bmatrix}, \quad (6)$$

$$S_y=\begin{bmatrix}-1 & -1 & -1\\ 0 & 0 & 0\\ 1 & 1 & 1\end{bmatrix}, \quad (7)$$

while the Scharr gradients, in the x and y directions, are given as:

$$S_x=\begin{bmatrix}-1 & 0 & 1\\ -3 & 0 & 3\\ -1 & 0 & 1\end{bmatrix}, \quad (8)$$

$$S_y=\begin{bmatrix}-1 & -3 & -1\\ 0 & 0 & 0\\ 1 & 3 & 1\end{bmatrix}. \quad (9)$$

Figures 3 and 4 show an example of salt boundaries detected by the Prewitt and the Scharr edge detectors. Figure 5 gives a comparison of Sobel, Prewitt, and Scharr edge detectors for salt dome detection. We can see that the boundary detected by the Sobel operator is very close to the ground truth. On the hand, the boundary detected by the Prewitt and Scharr edge detector deviate a bit from the ground truth. The better performance of the Sobel edge detector is due to the double weight on the center point. This increase in the weight helps in suppressing noise. The Scharr edge detector gives triple weight to the center point which reduces the effect of the neighboring points and therefore affect the accuracy as shown in Figure 5. The Sobel edge detector gives an optimal solution as it gives center point double the weight of neighboring point (Jin-Yu et al., 2009).

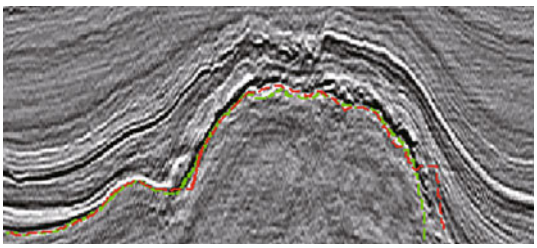

Fig.3 Salt boundary detected for Inline # 111 using the Prewitt edge detector.

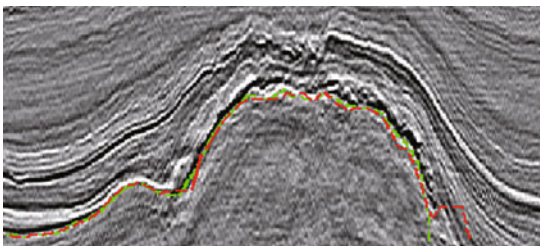

Fig.4 The salt boundary detected for Inline # 111 using the Scharr edge detector.

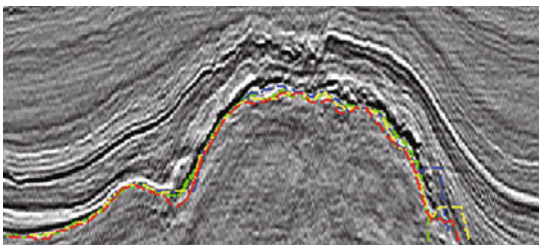

Fig.5 Ground truth (Green), 2D Sobel edge detector (Red), Prewitt edge detector (Blue), Scharr edge detector (Yellow).

Although the Sobel operator gives better results as compared to other edge detectors, considering the gradient map only in the x and y directions may not give accurate results along the diagonal directions of salt dome boundaries. Figure 6 shows the zoomed version of diagonal parts of the salt boundary detected by the Sobel edge detector. It can be seen that the detected boundary is not very close to the ground truth.

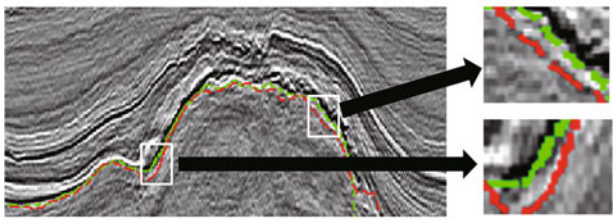

Fig.6 Zoomed portion of detected salt boundary using 2D Sobel edge detector without diagonal edges.

To improve the performance of the Sobel edge detector, we include the diagonal directions and the x and y directions. The discrete gradient equation for 3 × 3 Sobel edge detector in the diagonal directions are given as:

$$G_{45}=\{g(x+1,y)+2g(x+1,y+1)+g(x,y+1)\} -\{g(x,y-1)+2g(x-1,y-1)+g(x-1,y)\}, \quad (10)$$

$$G_{135}=\{g(x-1,y)+2g(x-1,y+1)+g(x,y+1)\} -\{g(x,y-1)+2g(x+1,y-1)+g(x+1,y)\}. \quad (11)$$

The convolution operators for the Sobel edge detector in the diagonal directions are given as:

$$S_{45}=\begin{bmatrix}-2 & -1 & 0\\ -1 & 0 & 1\\ 0 & 1 & 2\end{bmatrix}, \quad (12)$$

$$S_{135}=\begin{bmatrix}0 & -1 & -2\\ 1 & 0 & -1\\ 2 & 1 & 0\end{bmatrix}. \quad (13)$$

The magnitude of the total gradient is now computed as:

$$G=\sqrt{G_x^{\,2}+G_y^{\,2}+G_{45}^{\,2}+G_{135}^{\,2}}. \quad (14)$$

The 3D extension of the Sobel edge detector

For 3D seismic data, the Sobel operator on 2D slices is extended to 3D taking into account continuity in the medium. In the case of the 3D Sobel operator, the first mask (also called operator) detects discontinuity in the x direction, the second mask detects dissimilarity in the y direction, and the third mask detects dissimilarity in the z direction. The boundary of the salt dome is tracked by combining the three dissimilarity maps into a single magnitude map. In Figure 7, we show the 3D Sobel operators in x, y, and z directions which corresponds to crossline, inline, and time axes.

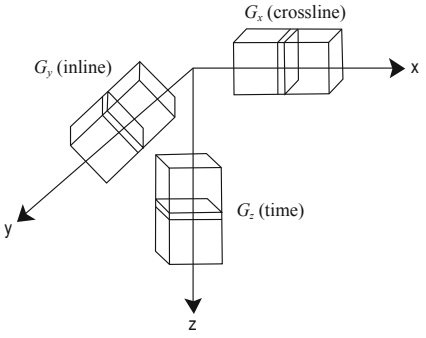

Fig.7 3D Sobel operator in the x, y, and z directions.

The size of 3D Sobel operator, used in our algorithm, for each direction is 3 × 3 × 3. The convolution operator for 3D Sobel edge detector in the x direction, y direction, and z direction is given as:

$$S_x(:,:,-1)=\begin{bmatrix}-1&0&1\\-2&0&2\\-1&0&1\end{bmatrix},\ S_x(:,:,0)=\begin{bmatrix}-2&0&2\\-4&0&4\\-2&0&2\end{bmatrix},$$

$$S_x(:,:,1)=\begin{bmatrix}-1&0&1\\-2&0&2\\-1&0&1\end{bmatrix}, \tag{15}$$

$$S_y(:,:,-1)=\begin{bmatrix}-1&-2&-1\\0&0&0\\1&2&1\end{bmatrix},\ S_y(:,:,0)=\begin{bmatrix}-2&-4&-2\\0&0&0\\2&4&2\end{bmatrix},$$

$$S_y(:,:,1)=\begin{bmatrix}-1&-2&-1\\0&0&0\\1&2&1\end{bmatrix}, \tag{16}$$

$$S_z(:,:,-1)=\begin{bmatrix}-1&-2&-1\\-2&-4&-2\\-1&-2&-1\end{bmatrix},\ S_z(:,:,0)=\begin{bmatrix}0&0&0\\0&0&0\\0&0&0\end{bmatrix},$$

$$S_z(:,:,1)=\begin{bmatrix}1&2&1\\2&4&2\\1&2&1\end{bmatrix}, \tag{17}$$

The magnitude of the total gradient is given as:

$$G=\sqrt{G_x^{\,2}+G_y^{\,2}+G_z^{\,2}}. \tag{18}$$

For the case of 2D Sobel edge detection, the Sobel operator in the x, y, and z directions may not produce accurate results for the diagonal parts of salt dome boundaries. We, therefore, introduce two more Sobel operators in the diagonal directions to detect the diagonal edges. The diagonal directions in 3D can be considered from different reference points, i.e. x, y, and z. We propose two 3D diagonal edge operators, S_{45} and S_{135}, by rotating S_x by 45° and 135°. The two proposed diagonal operators work well to overcome the problem of diagonal boundaries as shown in Figure 6. The convolution operators for the 3D Sobel in the diagonal directions are given as:

$$S_{45}(:,:,-1)=\begin{bmatrix}-2&-1&0\\-1&0&1\\0&1&2\end{bmatrix},\ S_{45}(:,:,0)=\begin{bmatrix}-4&-2&0\\-2&0&2\\0&2&4\end{bmatrix},$$

$$S_{45}(:,:,1)=\begin{bmatrix}-2&-1&0\\-1&0&1\\0&1&2\end{bmatrix}, \tag{19}$$

$$S_{135}(:,:,-1)=\begin{bmatrix}0&-1&-2\\1&0&-1\\2&1&0\end{bmatrix},\ S_{135}(:,:,0)=\begin{bmatrix}0&-2&-4\\2&0&-2\\4&2&0\end{bmatrix},$$

$$S_{135}(:,:,1)=\begin{bmatrix}0&-1&-2\\1&0&-1\\2&1&0\end{bmatrix}, \tag{20}$$

Based on this new formulation, the resulting magnitude of the total gradient is now obtained as:

$$G=\sqrt{G_x^{\,2}+G_y^{\,2}+G_z^{\,2}+G_{45}^{\,2}+G_{135}^{\,2}}. \tag{21}$$

Experimental results

We used our salt dome detection method to data acquired from the Netherlands offshore F3 block in the North Sea. The dataset is real and covers a block of 24 x 16 km2. The Inline range (or slice number) is from 100 to 750, the cross line range (or slice number) is 300 to 1250, and the time direction ranges from 0 to 1848 ms. The ground truth for the data is labeled manually by experts from the Geoscience department at KFUPM.

In the first step, we used the normalization scheme to enhance the salt dome edges in the dataset. Then, we used the 3D Sobel edge detector to delimit the salt boundaries. The thresholding step in 3D edge detection leaves many disconnected and noisy regions. To connect the disconnected regions and to remove the noisy regions, we use two basic morphological operations, i.e. dilation followed by erosion. Dilation process enlarges the region of salt boundaries, and this helps in connecting the disconnected regions. Erosion process shrinks the regions and helps in removing noisy patches.

Inline # 111 is considered as a test case to compare the performance of the proposed 3D salt dome detection method with the conventional 2D Sobel edge detector based method. Figure 8 provides a comparison of the 2D Sobel edge detector and the proposed 3D Sobel edge detector. The green boundary here is the ground truth, red is the boundary produced by the proposed method, and blue is the boundary produced by the 2D Sobel edge detector. We see that the proposed method is able to outline the boundary with excellent accuracy. Figure 9 shows the boundary points using the proposed method, the 2D Sobel edge detector, and the ground truth points. We can see that the boundary produced by our algorithm is very close to the ground truth. The boundary produced by the 2D Sobel edge detector based method loses the track at many points along the diagonal boundaries.

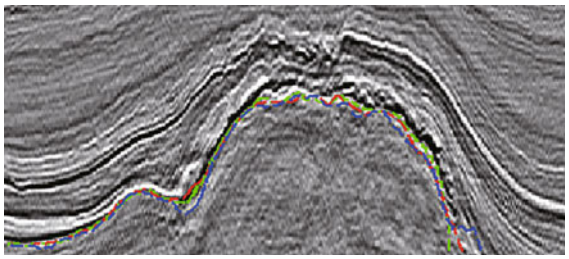

Fig.8 Ground truth (Green), Salt boundary detected for Inline # 111 using the proposed method (Red), boundary detected for Inline # 111 using the 2D Sobel edge detector (Blue).

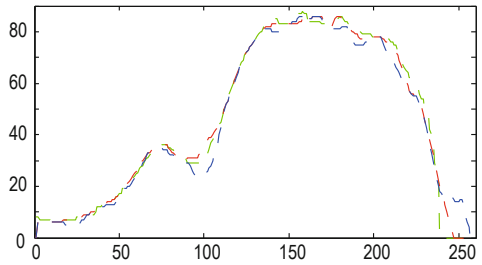

Fig.9 Ground truth points (Green), salt boundary points using the proposed method (Red), salt boundary points using the 2D Sobel edge detector (Blue).

In Figure 10, we show the salt boundary detected for the seismic volume (80 Inlines) using the proposed method. The proposed algorithm gives excellent results even for the Inlines which have an uneven salt boundary.

We compared the performance of proposed method with the 2D Sobel edge detector based salt dome detection method (Jing et al., 2007), the 3D Sobel edge detector based method (Aqrawi et al., 2011), and the texture attributes based method (Berthelot et al., 2012). For the texture attributes based method (Berthelot et al., 2012), GLCM based features, eigen structure based features and Gabor filter based attributes were used.

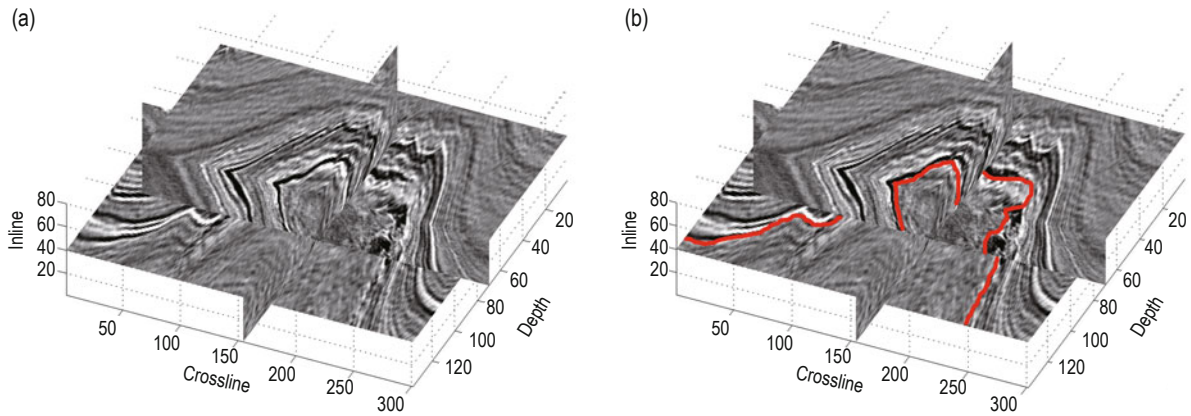

Fig.10 (a) Seismic volume containing 80 Inlines. (b) Salt boundary detected for the seismic volume using the proposed method.

Figure 11 shows the results of the salt boundary detected using the three methods, namely the 2D Sobel based method, the 3D Sobel based method, and the texture based method, together with our proposed method. The green boundary here is the ground truth, red is the boundary produced by the proposed method, blue is the boundary produced by the 2D Sobel based method, yellow is the boundary produced by the Aqrawi's 3D Sobel based method, and pink is the boundary produced by texture based method. We can see that the results obtained using the proposed algorithm outperforms all other methods (see also Figure 12). We can see that the boundary produced by our algorithm is very close to the ground truth. Jing et al. (2007) and Aqrawi et al. (2011) methods are not able to trace the boundary accurately along the diagonals. Berthelot et al. (2012) deviates from the ground truth at multiple points especially at the start and at the end of the salt dome boundary as expected for texture based techniques. Figure 13 shows the zoomed version of the diagonal parts of salt dome boundary for Inline # 111. We can see that our algorithm performs better than other edge detection based techniques which fails to trace the boundary accurately along the diagonals.

Finally, we also show in Table 1 the average classification accuracy for Inlines # 111 to 134 (24 slices) using the proposed method, the 2D Sobel based method, the 3D Sobel based method, and the texture based method. The proposed method gives an average accuracy of 89% which is 8% higher than the 2D Sobel based method, 4% higher than the 3D Sobel based method, and 2% higher than the texture based method (which is computationally very expensive).

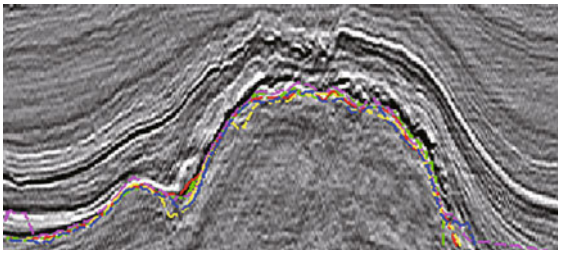

Fig.11 Salt boundary detected for Inline # 111: Proposed method (Red), 2D Sobel based method (Blue), 3D Sobel based method (Yellow), Texture attributes based method (Pink), Ground truth (Green).

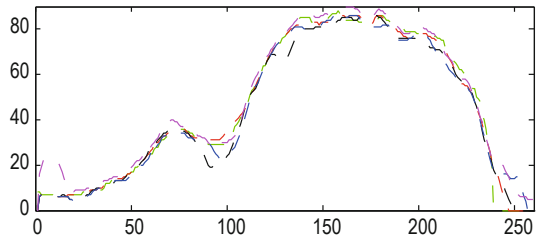

Fig.12 Salt boundary points detected for Inline # 111: Proposed method (Red), 2D Sobel based method (Blue), 3D Sobel based method (Black), Texture attributes based method (Pink), Ground truth (Green).

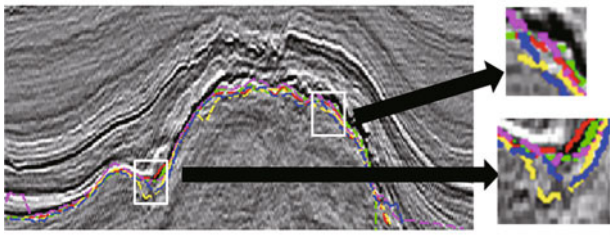

Fig.13 Zoomed portion of diagonal salt boundary for Inline # 111: Proposed method (Red), 2D Sobel based method (Blue), 3D Sobel based method (Yellow), Texture attributes based method (Pink), Ground truth (Green).

Table 1 Classification Accuracy (averaged over 24 slices)

Salt Dome Detection Method	Accuracy
Proposed method	89.64%
2D Sobel based (Jing et al., 2007)	81.13%
3D Sobel based (Aqrawi et al., 2011)	85.22%
Texture attributes based (Berthelot et al., 2012)	87.78%

Precision, Recall and F-measures have also been used traditionally as evaluation metrics in image segmentation. To measure these metrics, we compute the True Positive (*TP*), the False Positive (*FP*), the True Negative (*TN*), and the False Negative (*FN*) using the ground truth and the detected salt region. Precision, recall, and F-measure are computed using:

$$Precision = \frac{TP}{TP + FP}, \tag{22}$$

$$Recall = \frac{TP}{TP + FN}, \tag{23}$$

$$F - Measure = 2 \times \frac{Precission \times Recall}{Precission + Recall}. \tag{24}$$

In Figure 14, we show the ground truth of the salt dome and the salt regions detected using the proposed method, 2D Sobel based method, 3D Sobel based method, and the texture based method for Inline # 111. In table-2, we show the average precision, recall, and F-measure values computed for Inlines # 111 to 134. The F-measure value obtained for the proposed method

is almost 3% higher than Jing and Aqrawi's method and 4% higher than the texture attributes based method. The results show the improved performance obtained using the proposed algorithm while keeping the algorithm complexity to the minimum.

Table 2 Precision, Recall & F-Measure

Salt Dome Detection Method	Precision	Recall	F-Measure
Proposed method	98.66	97.64	98.15
2D Sobel (Jing et al. (2007))	97.68	94.71	95.17
3D Sobel (Aqrawi et al. (2011))	98.60	93.99	95.24
Texture attributes Berthelot et al. (2012))	92.88	98.86	94.78

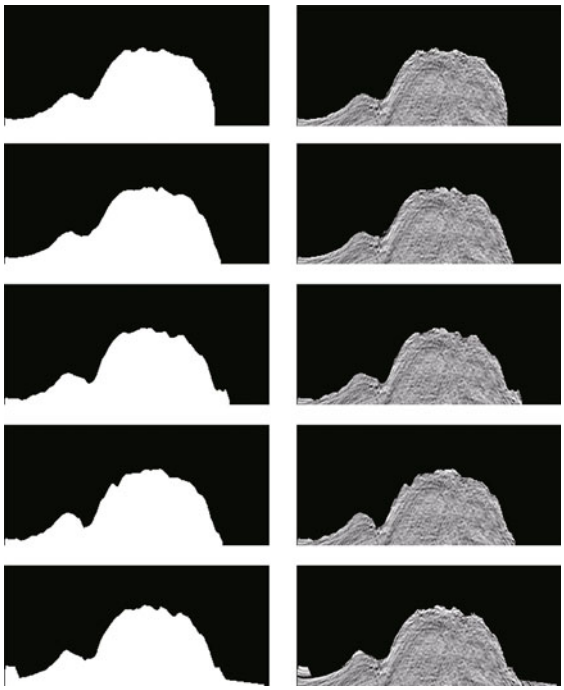

Fig.14 1st Row: Ground Truth, Detected salt dome region: The proposed method (2nd Row), 2D Sobel based method (3rd Row), 3D Sobel based method (4th Row), Texture attributes based method (5th Row).

To further illustrate the performance of the proposed algorithm, Figure 15 shows the detected salt volume using the proposed approach. The algorithm results in a relatively smooth profile as expected in practical scenarios. The final salt profiles obtained using our algorithm are very encouraging. The results are very close to the ground truth, as such, the resulting salt profile can be very useful in different practical scenarios and applications.

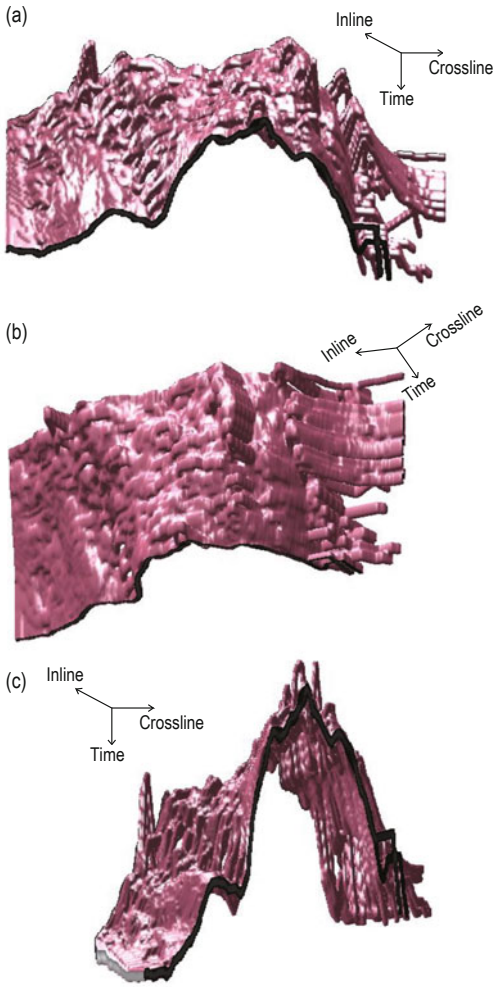

Fig.15 3D Salt Dome detected using the proposed method.

Conclusions

We introduced a new approach for salt dome detection using a 3D multidirectional edge detector. To identify the boundaries of salt domes, the algorithm combines 3D gradient maps computed along diagonal directions and those computed along the x, y, and z directions. By combining the diagonal edges with the edges in the x, y, and z directions, we ensure excellent detection accuracy even when the salt boundaries are represented by very weak reflectors. We tested the proposed approach on the Netherlands offshore F3, block and showed that the proposed algorithm detected salt bodies with excellent accuracy and outperformed existing techniques. More importantly, the low computational complexity of the proposed algorithm makes it suitable for real time implementation and deployment.

Acknowledgments

The work presented in this paper has been supported by the Center for Energy and Geo Processing (CeGP) at King Fahd University of Petroleum & Minerals (KFUPM), under Project no. GTEC 1401-1402. We would like to thank the anonymous reviewers for their excellent feedback and comments that helped in improving the overall structure and clarity of the paper.

References

Aqrawi, A. A., Boe, T. H., and Barros, S., 2011, Detecting salt domes using a dip guided 3d sobel seismic attribute: 81th Annual International Meeting, SEG, Expanded Abstracts.

Berthelot, A., Solberg, A. H., and Gelius, L. J., 2013, Texture attributes for detection of salt: Journal of Applied Geophysics, **88**, 52 – 69.

Berthelot, A., A., Solberg, H. S., Morisbak, E., and Gelius, L. J., 2012, 3d segmentation of salt using texture attributes: 87th Ann. Internat. Mtg, Soc. Expl. Geophys., Expanded Abstracts, 1–5.

Brown, A. R., Brown, A. R., Brown, A. R., and Brown, A. R., 2004, Interpretation of three-dimensional seismic data: American Association of Petroleum Geologists Tulsa.

Gonzalez, R. C., and Richard, E., 2002, Woods, digital image processing: ed: Prentice Hall Press, ISBN 0-201-18075-8.

Hauks, J., Ravndal, O. R., Fotland, B., Bounaim, A., and Sonneland, L., 2013, Automated salt body extraction from seismic data using the level set method: First Break, **31**, 35–P42.

Hegazy, T., and AlRegib, G., 2014, Texture attributes for detecting salt bodies in seismic data: 89th Ann. Internat. Mtg, Soc. Expl. Geophys., Expanded Abstracts, 1455–1459.

Jing, Z., Z., Yanqing, Z., Zhigang, C., and Liu, J. H., 2007, Detecting boundary of salt dome in seismic data with edge detection technique: 77th Ann. Internat. Mtg, Soc. Expl. Geophys.,Expanded Abstracts, 1392–1396.

Li, L. L., Han, L. G., and Huang, D. N., 2014, Normalized edge detection, and the horizontal extent and depth of geophysical anomalies: Applied Geophysics, **11**, 149–157.

Lomask, J., and Biondi, B., 2003, Image segmentation for tracking salt boundaries: Stanford exploration: Project report, 193200.

Lomask, J., Biondi, B., and Shragge, J., 2004, Image segmentation for tracking salt boundaries: 74th Annual International Meeting, SEG, Expanded Abstracts, 2443–2446.

Lomask, J., Clapp, R. G., and Biondi, B., 2006, Parallel implementation of image segmentation for tracking 3d salt boundaries: Presented at the 68th Annual International Meeting, EAGE, Expanded Abstracts.

Shi, J., and Malik, J., 2000, Normalized cuts and image segmentation: IEEE Transactions on Pattern Analysis and Machine Intelligence, **22**(8), 888–905.

Wang, J., Chen, Y., Xu, D., and Qiao, Y., 2009, Structure oriented edge-preserving smoothing based on accurate estimation of orientation and edges: Applied Geophysics, **6**, 367–376.

Xu, M. L., Yang, C. B., Wu, Y. G., Chen, J. Y., and Huan, H. F., 2015, Edge detection in the potential field using the correlation coefficients of multidirectional standard deviations: Applied Geophysics, **12**, 23–34.

Zhang, J. Y., Chen Y., and Huang, X. X., 2009, Edge detection of images based on improved sobel operator and genetic algorithms: Proceedings on Image Analysis and Signal Processing, IEEE, 31–35.

Zhang, Y., and Halpert, A., 2012, Enhanced interpreter-aided salt boundary extraction using shape deformation: 87th Ann. Internat. Mtg, Soc. Expl. Geophys., Expanded Abstracts, 1–5.

Asjad Amin received the B.S. degree in telecommunication engineering from the National University of Computer & Emerging Sciences NU-FAST, Islamabad, Pakistan in 2007 and M.S. degree in electrical engineering from University of Engineering & Technology, Taxila, Pakistan in 2012. Since 2012, he is with the department of electrical engineering at King Fahd University of Petroleum & Minerals, Saudi Arabia, where he is working towards his Ph.D. He joined the Islamia University of Bahawalpur, Pakistan, as Lecturer in 2008. His research interests include image and video processing, seismic imaging and modeling, machine learning, and image segmentation. Email: asjad@kfupm.edu.sa

Dr. Mohamed Deriche received his MS and PhD from U. of Minnesota in 1994. He then joined Queensland University of Technology, Australia. In 2001, he joined the EE Department at King Fahd University of Petroleum & Minerals, where he led the signal processing. He has published over 200 papers in multimedia signal and image processing. He delivered numerous invited talks. He chaired several conferences including TENCON, GLOBALSIP-MPSP, IEEE GCC, IPTA. He supervised over 30 MSc and PhD students. He received the IEEE third Millennium Medal, Shauman award from best researcher, excellence in research and excellence in teaching awards at KFUPM.